Comparative Study of Electrical Machines with Soft Magnetic Composite Cores

***Abstract*— In this paper, various kinds of electrical machines with soft magnetic composite (SMC) cores are compared, based on the qualitative and quantitative comparison methods. In the first part, the performances of five typical electrical machines with SMC cores are qualitatively compared. Simplified power equations for transverse flux, axial flux and radial flux electrical machines are deduced to show the main difference among them and key design points of each machine. In the second part, the outer rotor claw pole machine (CPM) and outer rotor transverse flux machine (TFM) are comprehensively compared in quantitative way, based on the 3D finite element method (FEM). It shows that the power capability of the outer rotor CPM is much higher than that of the TFM. On the other hand, the outer rotor CPM has higher cogging torque and no-load losses than the TFM. Furthermore, the four outer rotor radial flux machines are optimized and compared with the outer rotor CPM. The calculated results of the outer rotor TFM are compared with the experiment results, showing that the analysis results match well with the experiment ones. Several useful and interesting conclusions have been obtained for the electrical machines with SMC cores.**

***Index Terms*— Electrical machines, soft magnetic composite (SMC), qualitative and quantitative comparison, claw pole motor, transverse flux motor, radial flux machine, finite element method (FEM)**

I. Introduction

SOFT magnetic composite (SMC) material is a relatively new soft magnetic material that is composed of surface electrically insulated iron powder particles, which results in low eddy current loss, and magnetic and thermal isotropy. As the eddy current loss of the SMC is much lower than that of electrical laminated steels, especially at the higher frequency, its total core loss can be comparable to, or lower than that of the electrical laminated steels at a higher frequency, e.g. over 300 Hz. Thus, it is suggested that SMC is suitable for higher frequency applications, such as the high speed electrical machines and electrical machines with large number of pole pairs. Due to the magnetic and thermal isotropy, SMC is suitable for designing the 3D magnetic flux electrical machines with a quite high freedom. Therefore, various kinds of novel electrical machines can be manufactured, such as the transverse flux machine (TFM) [1], claw pole machine (CPM) [2, 3] and axial flux machine (AFM) [4, 5]. They are difficult to be designed with electrical steels. As manufactured by the high purity iron powder, the SMC material has high magnetic saturation. It has a number of advantages over the traditional electrical steels such as 3D isotropic magnetic properties and relatively low core losses in the high frequency applications.

By using the powder metallurgical technology, the electrical machines with SMC cores can be manufactured in a convenient and economical way. In the commercial production, the motor components with SMC can be produced by punching the SMC powders in the molds with the pressing machine. After the compaction process, the SMC component will be heat treated for relieving the mechanical stress. There is no any further machining process needed on the SMC components. Compared with the manufacturing process of the electrical machines with sheet steels, the manufacturing costs of SMC motors can be quite low. Moreover, motors with SMC cores have very low material waste (less than 5%) during the manufacturing process. It also has the merits of the net shape, smooth surface and good tolerances for the electrical machines [6, 7].

Therefore, SMC material brings a great of potential for the electrical machine design and commercial production. During the last two decades, various researches have put great efforts on designing electrical machines with this material. It includes the novel motor topology with SMC core, the core loss modeling, performance analysis, optimization and etc. [8-14].

On the other hand, SMC cores have the following disadvantages: (1) lower permeability compared to laminated steels, (2) higher hysteresis loss, and (3) low mechanical strength, especially when the low mass density production is applied. To alleviate these disadvantages, some measures should be taken. Firstly, the permanent magnet (PM) excitation can be used in the electrical machines with SMC cores, because PM machines are not sensitive to the permeability of the material. Secondly, the operational electrical frequency of the electrical machine with SMC cores should be relatively high, as the hysteresis loss is proportional to the frequency and the eddy current loss is proportional to the square of frequency. Thus, the total core loss can be lower than the electrical steel at high frequency. Thirdly, different mass density cores can be considered to meet the performance requirements, including the electromagnetic performance and mechanical strength requirements. Compared with the material cost of the electrical machine with sheet steels, the manufacturing cost with reasonable press machine can be quite low.

During the past decades, various electrical machines with SMC cores were designed for different applications. Most of them are for home applications [15-17]. By utilizing the advantages of the SMC material, the electrical machines with SMC cores can output better performance than the machines with electrical steels [1, 18]. In [1], A TFM with SMC stator was compared with two commercial motors of laminated cores, a high efficiency induction motor and a radial field brushless DC servo motor, with rated torques ranged from 3.4 to 3.7 Nm. Through the comparison, it can be seen that the proposed SMC motor features a torque per unit volume of 4.5 times that of the laminated induction motor. Meanwhile, it delivers 2.25 times the torque per unit volume of the brushless DC servo motor. In [18], the induction machine with SMC cores can be optimized and has better performance than the initial machine. In addition, the wedges made by SMC material can be used to improve the performance of axial flux electrical machines with laminated steels [19]. Recently, the electrical machines with SMC cores for the application in electric vehicles have been presented, such as the axial flux permanent magnet machine and transverse flux reluctance machine [20-22].

This paper presents a comparative study of electrical machines with SMC cores. Various electrical machines with SMC core are discussed. A basic performance comparison among them will be presented, which includes the torque density, power density and efficiency. A qualitative comparison among the general electrical machines, including the AFM, TFM, and radial flux machine (RFM), will be conducted based on the simplified magnetic model. Thereafter, two potential electrical machines, namely outer rotor CPM and outer rotor TFM, will be chosen to compare quantitatively.

II. Comparison of Electrical Machines with SMC Cores

To have a qualitative understanding on that which kinds of topologies are suitable for developing electrical machines with the SMC cores, five typical electrical machines with SMC cores have been chosen and compared. Motor *A* is a CPM with an inner rotor which was prototyped by utilizing the low pressure compaction in the mold, as shown in Fig. 1(a) [3]. Motor *B* is a TFM with an outer rotor, which was prototyped by using the wire cutting of an SMC preform [1], as shown in Fig. 1(b). Motor *C* is a CPM with an outer rotor, which was prototyped by using the wire cutting method [15], as shown in Fig. 1(c). These motors belong to the 3-D magnetic flux electrical machines with the global winding configurations, and they are all prototyped in the Center for Electrical Machines and Power Electronics (CEMPE), University of Technology Sydney. Motor *D* is an axial flux PM generator [16]. Motor *E* is a radial flux PM synchronous machine (PMSM) with improved 3-D flux structure, which was developed for comparison with the commercial PMSM with electrical steels [17]. It utilizes the magnetic isotropy of SMC, and the flux of this motor is 3D. The machine has gained much performance improvement compared with the conventional PMSM with electrical steels.

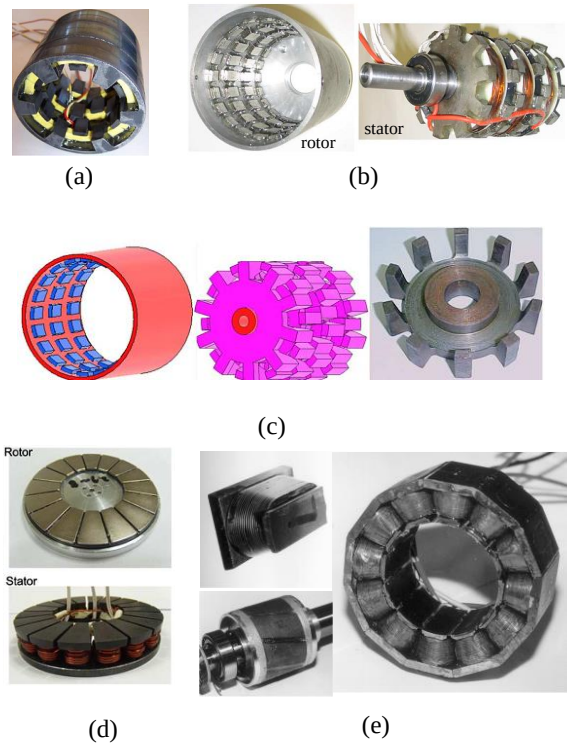

Fig. 1. Photos of motors, (a) motor A: inner rotor claw pole motor with low density mold [3], (b) motor B: outer rotor transverse flux motor [1], (c) motor C: outer rotor claw pole motor [15], (d) motor D: axial flux generator [16], and motor E: radial flux motor [17].

TABLE I
PERFORMANCE OF ELECTRICAL MACHINES WITH SMC CORE

		Motor A	Motor B	Motor C	Motor D	Motor E
performance	Rated torque/current density (Nm, A/mm^2)	0.2/3.3	3.4/5.5	3/3.25	0.28/3.0	4.6/(100 °C)
	Rated power/current density (W, A/mm^2)	62/3.3	640/5.5	560/3.25	66/3.0	1,445/(100 °C)
	Rated frequency (Hz)	300	300	300	267	300
	Rated efficiency (%)	63	79.5	76	84	92
volume	Outer radius of effective magnetic parts (mm)	34	47	50	40.5	53.5
	Axial length of the effective parts (mm)	55	93	108	21	55
	Volume (mm^3)	199,742	645,399	848,230	108,213	494,561
	Torque per unit volume (Nm/m^3)	1,000	5,268	3,536	2,587	9,400

Table I tabulates the basic performance of these five motors, including the rated torque subject to the limit of current density or temperature rise, rated power, rated efficiency, and torque per unit volume. It can be seen that the rated frequency of these

motors is around 300 Hz, which can achieve a comparative core loss characteristic as that of laminated steel machines. Because of the rated torque or power is determined by the electrical load, the limits of current density or temperature rise of each motor are also listed in this table.

By comparing the performances of these motors, it can be found that the torque per unit volume of motor *E* is 9,400 Nm/m^3, which is the highest one. However, this result is achieved under the constraint that the temperature rise of armature coil is 100 °C. Nevertheless, the other motors are operated at much lower temperature rise than 100 °C. Thus, to compare them fairly, some design considerations and design differences among these motors should be considered. Motor *E* is a 3-D radial flux motor designed by Jack, *et al.* [17].

To improve the performance of the machines with SMC core, some special measures have been taken on this motor when compared with the commercial laminated PMSM. Firstly, the core back and core teeth are extended, and the slot fill factor is increased by utilizing the round corner characteristic of the molded SMC teeth. Secondly, the rated torque is obtained with the temperature rise of 100 °C in the coil. Lastly, the SMC core is pressed at 800 Mpa. Compared with the laminated commercial PMSM, the motor with SMC core shows better performance. As reported in [17], the torque per unit volume of the motor with powder iron core is 9,400 Nm/m^3, while the torque per unit volume of the commercial motor is 3,600 Nm/m^3. The temperature rises of the motors *A*, *B* and *C* are around 66 °C, and their slot fill factors are 0.65, 0.5, and 0.32, respectively. As shown in Table I, motor *A* has relatively low torque per unit volume, because the SMC core used in this motor is pressed at 179 Mpa. It was reported that the CPM with high density (7.2 g/cm^3) SMC core has 18 % better performance than that with low density (5.8 g/cm^3) core [3]. On the other hand, the CPM and TFM have the merits of high slot fill factor capability due to their inherent structures of global winding. Thus, some appropriate assumptions should be taken to compare the torque capability of these motors fairly. The slot fill factors of the motors *A*, *B*, and *C* will be increased to 0.75, with comparable powder mass density (7 g/cm^3), and the same operation temperature rise of 66 °C for that of motor *E*.

Table II tabulates the performance comparison with the assumption of the same conditions that the temperature rise is around 66 °C and the slot fill factor is 0.75. It can be found that motor *C* has the highest specific torque (torque per unit volume), motor *B* has the second highest, and motor *A* has the lowest.

TABLE II
COMPARISON OF ELECTRICAL MACHINES WITH COMPARABLE CONDITIONS

Item	Motor A	Motor B	Motor C	Motor D	Motor E
Specific torque (Nm/m^3)	1,000	5,268	3,536	2,587	6,539
Slot fill factor	0.65	0.5	0.32	-	0.61
New specific torque (Nm/m^3)	1,361	7,902	8,287	-	8,039
New slot fill factor	0.75	0.75	0.75	-	0.75

Besides the electromagnetic performance of these motors, the structure of TFM and CPM is more complex than that of the radial flux and axial flux motors. Thus, using SMC core can reduce the manufacturing cost. In addition, the global winding used in the transverse flux motor and claw pole motors has no end regions, which can reduce the copper material cost and excessive copper loss.

In this section, five typical electrical machines with SMC cores developed lately are listed and compared. It shows that the outer rotor CPM and outer rotor TFM have better performance, while motor *A*, the inner rotor CPM has the lowest specific torque. Thus, it is necessary to further investigate the principles and design techniques for the electrical machines.

III. QUALITATIVE COMPARISON OF RADIAL FLUX, TRANSVERSE FLUX, AND AXIAL FLUX MOTOR

In the design of electrical machines with SMC cores, the AFM and RFM with concentrated winding configuration and TFM have been widely investigated [10, 22-25]. In this section, the differences among RFM, TFM, and AFM will be compared, based on the simplified power equation. The design principles of them will be developed, including the electromagnetic torque with respect to the ratio of axial length to the outer radius.

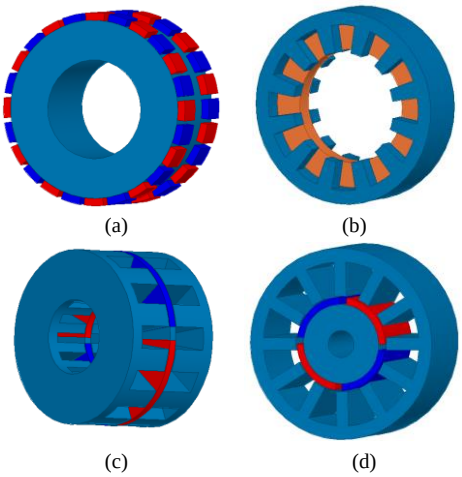

Fig. 2. Topologies of PMSM: (a) rotor for TFM, (b) stator and coil for TFM, (c) AFM, and (d) RFM.

Fig. 2 shows the main magnetic parts of TFM, AFM and RFM. The TFM is an inner rotor machine. The AFM is a machine with one inner rotor between two stator cores. The winding for the AFM and RFM is of the concentrated type.

For the general PM machines, the main electromagnetic relationships can be expressed by the following equations. The differences among TFM, AFM and RFM are the flux linkage per turn and the area of coil window. In this paper, the optimum brushless DC (BLDC) model is used, in which the phase current is controlled to have the same phase angle as the phase back electromotive force (*emf*). The electromagnetic power of the PM machine can be expressed as

$$P_{em} = \frac{m}{T}\int_0^T e(t)i(t)dt = \frac{m}{T}\int_0^T E_m \sin(\frac{2\pi}{T}t) I_m \sin(\frac{2\pi}{T}t)dt = \frac{m}{2}E_m I_m \quad (1)$$

where m is the number of phases, T the electrical period, E_m the magnitude of phase back emf, and I_m the magnitude of phase current. The back emf can be expressed as

$$e_m = N_{coil}\frac{d\varphi}{dt} = N_{coil}\varphi_m \frac{2\pi}{T}\sin(\frac{2\pi}{T}t) \quad (2)$$

where N_{coil} is the number of turns per phase, and φ the flux per turn, which can be expressed as

$$\varphi = -\varphi_m \cos(\frac{2\pi}{T}t). \quad (3)$$

The electrical angular speed can be expressed as

$$\omega_e = \frac{2\pi}{T} = P_r \omega_r \quad (4)$$

where P_r is the number of rotor pole pairs, and ω_r the mechanical angular speed. The phase current can be expressed as

$$I_m = A_c J_m \quad (5)$$

where A_c is the cross-sectional area of the coil, and J_m the current density (magnitude value). The number of turns per phase can be expressed as

$$N_{coil} = \frac{N_s}{m}\frac{K_{sf}A_s}{A_c} \quad (6)$$

where N_s is the number of slots, K_{sf} the slot fill factor, and A_s the slot area. By combining the above equations and ignoring the stator resistance loss, the output power can be expressed as

$$P_{out} = \eta P_{em} = \eta\frac{m}{2}N_{coil}P_r\omega_r\varphi_m I_m \quad (7)$$

where η is the efficiency. The output torque can be expressed as

$$T_{out} = \frac{P_{out}}{\omega_r} = \eta\frac{m}{2}P_r\varphi_m K_{sf}\frac{N_s}{m}A_s J_m \quad (8)$$

To simplify the analysis, the torque capability can be expressed by the electromagnetic torque

$$T_{em} = \frac{N_s}{2}P_r\varphi K_{sf}A_s J_m \quad (9)$$

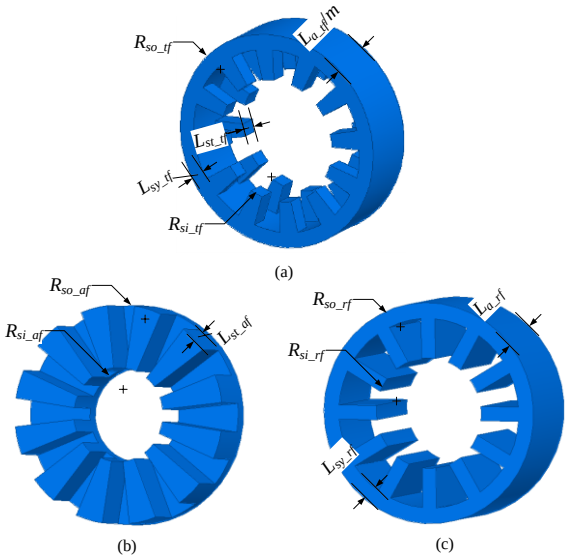

Fig. 3. Main dimensions of the TFM, AFM and RFM

Fig. 3 shows the main dimensions of TFM, AFM and RFM. They will be used to deduce the main electromagnetic torque of these machines.

A. Transverse Flux Motor

The electromagnetic torque of TFM can be expressed as

$$T_{tf} = C_{T\_tf}(\frac{L_{a\_tf}}{m} - 2L_{st\_tf})L_{st\_tf}(R_{so\_tf} - R_{si\_tf} - L_{sy\_tf})R_{si\_tf}J_m \quad (10)$$

where

$$C_{T\_tf} = 0.5\pi N_{s\_tf} m K_{sp\_tf} K_{c\_tf} K_{d\_tf} B_{g\_tf} k_{sf\_tf} \quad (11)$$

where L_{a_tf} is the effective axial length, m the number of phases, L_{st_tf} the stator tooth length in the axial direction, R_{so_tf} the stator outer radius, R_{si_tf} the stator inner radius, L_{sy_tf} the length of stator yoke, N_{s_tf} the number of stator poles, K_{sp_tf} the ratio of stator tooth width to pole arc, K_{c_tf} the winding factor, K_{d_tf} the flux leakage coefficient, B_{g_tf} the air gap flux density, and k_{sf_tf} the slot fill factor.

Based on (10), when the following conditions are met,

$$L_{st\_tf} = \frac{1}{4}\frac{L_{a\_tf}}{m} \quad (12)$$

$$R_{si\_tf} = \frac{1}{2}(R_{so\_tf} - L_{sy\_tf}) \quad (13)$$

the electromagnetic torque reaches the maximum, which has the form as,

$$T_{tf} = \frac{C_{T\_tf}}{32}(\frac{L_{a\_tf}}{m})^2(R_{so\_tf} - L_{sy\_tf})^2 J_m \quad (14)$$

By defining the ratio of axial length to outer radius of motor (λ), for a given volume (V) and λ, the outer radius of the machine can expressed as,

$$R = \sqrt[3]{V/2\pi\lambda} \quad (15)$$

Thus, it can be found that the torque per unit volume has the following relationship with respect to the λ and V,

$$T_{tf}/V \propto \sqrt[3]{V\lambda^2} \quad (16)$$

B. Axial Flux Motor

The electromagnetic torque of AFM can be expressed as,

$$T_{af} = 2C_{T\_af}(R_{so\_af}{}^2 - R_{si\_af}{}^2)(R_{so\_af} + R_{si\_af})L_{st\_af}J_m \quad (17)$$

where

$$C_{T\_af} = \frac{N_{r\_af}}{4N_{s\_af}}\pi^2(1-K_{sp\_af})K_{sp\_af}B_{g\_af}k_{sf\_af}K_{c\_af}K_{d\_af} \quad (18)$$

where R_{so_af} is the stator outer radius, R_{si_af} the stator inner radius, L_{st_af} the length of the stator slot in the axial direction, N_{r_af} the number of rotor poles, N_{s_af} the number of stator slots, K_{sp_af} the ratio of slot width with respect to pole arc, B_{g_af} the air gap flux density, K_{sf_af} the slot fill factor, K_{c_af} the winding factor, and K_{d_af} the flux leakage factor.

By analyzing the torque equation (17), it can be found that if the R_{so_af} and R_{si_af} satisfy

$$R_{so\_af} = 3R_{si\_af} \quad (19)$$

the electromagnetic torque reaches the maximum, and it can be expressed as

$$T_{af} = \frac{64C_{T\_af}}{27}R_{so\_af}{}^3L_{st\_af}J_m \quad (20)$$

Thus, the torque per unit volume of the AFM with respect to volume and λ has the form as,

$$T_{af}/V \propto \sqrt[3]{V/\lambda} \quad (21)$$

C. Radial Flux Motor

The electromagnetic torque of RFM can be expressed as,

$$T_{rf} = C_{T\_rf}(R_{so\_rf} - L_{sy\_rf} - R_{si\_rf})(R_{so\_rf} - L_{sy\_rf} - (1-2K_{sp\_rf})R_{si\_rf})R_{si\_rf}L_{a\_rf}J_{m\_rf} \quad (22)$$

where

$$C_{T\_rf} = \frac{N_{r\_rf}}{2N_{s\_rf}}B_{g\_rf}\pi^2K_{sf\_rf}K_{d\_rf}K_{c\_rf}K_{sp\_rf} \quad (23)$$

where R_{so_rf} is the stator outer radius, L_{sy_rf} the length of the stator yoke, R_{si_rf} the stator inner radius, K_{sp_rf} the ratio of stator tooth width to the pole arc, L_{a_rf} the axial length of stator core, B_{g_rf} the air gap flux density, K_{sf_rf} the slot fill factor, K_{d_rf} the flux leakage factor, K_{c_rf} the winding factor, N_{r_rf} the number of rotor poles, and N_{s_rf} the number of stator slots.

By analyzing the torque equation, it can be found that when the R_{si_rf}, R_{so_rf}, L_{sy_rf} and K_{sp_rf} can meet the following constraints,

$$R_{si\_rf} = K(R_{so\_rf} - L_{sy\_rf})$$
$$K = \frac{4-4k_{sp\_rf}}{3(1-2k_{sp\_rf})} - \sqrt{\left(\frac{2-2k_{sp\_rf}}{3(1-2k_{sp\_rf})}\right)^2 - \frac{1}{3(1-2k_{sp\_rf})}} \quad (24)$$

the torque reaches the maximum (where we assume that the k_{sp_rf} equals 0.5) and it can be expressed as

$$T_{rf} = C_{T\_rf}\frac{1}{4}(R_{so\_rf} - L_{sy\_rf})^3L_{a\_rf}J_m \quad (25)$$

Thus, the torque per unit volume of the RFM with respect to volume and λ, has the form as,

$$T_{rf}/V \propto \sqrt[3]{V/\lambda} \quad (26)$$

By analyzing the power equations of TFM, AFM, and RFM, several important conclusions can be obtained as follows.

Firstly, it can be concluded from equation (10) that the torque of TFM is proportional to the number of stator poles, and from (16) the torque per unit volume is proportional to the two thirds root of the ratio of the effective axial length to the outer radius of the motor, and one third root of the volume. The torque of the TFM will be maximized when the width of the stator tooth in the axial direction equals a quarter of the axial length of one disk, and the stator inner radius equals half the difference between the stator outer radius and the length of the stator yoke in the radial direction.

For the AFM, based on (17), its torque is proportional to the number of rotor poles divided by the number of stator slots, and based on (21), its torque per unit volume is inversely proportional to one third root of effective axial length to the outer radius of the motor and proportional to one third root of the volume. The torque of the AFM will be maximized when the outer radius of the motor is three times the inner radius.

For the RFM, its torque has the same relationship as that of the AFM as shown in (22) and (26). When the dimensions of the RFM meet (24), the torque of RFM will be maximized.

TABLE III
RATIO OF AXIAL LENGTH TO OUTER RADIUS

Item	Motor A	Motor B	Motor C	Motor D	Motor E
Ratio of the axial length to outer radius	1.6	1.97	2.16	0.5	1.03

Table III lists the ratio of effective axial length to the outer radius for all motors. As discussed above, the torque of the TFM is proportional to the two thirds root of ratio of axial length to outer radius; the λ of motor *A* is lower than motor *B* and motor *C*. It is one of the reasons that the torque per unit volume of motor *A* is the lowest one; another reason is that the volume of motor *A* is relatively smaller than that of *B* and *C*. The third reason is that motor *A* has chosen the inner rotor topology, which makes the effective air gap radius lower than that of the motor with outer rotor. Therefore, depending on the dimension requirements, all the AFM, RFM and TFM can be chosen. Considering the high torque per unit volume for the long axial length application and low cost manufacturing (module design and small pressing tons), in the electrical machines with SMC core, the TFM and CPM may be the better choices and they are preferred to be designed with outer rotor topology, large number of pole pairs, and relatively large λ.

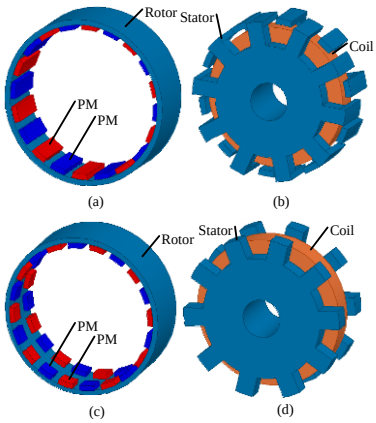

Fig. 4. Magnetic relevant parts of one stack of CPM and TFM, where (a) the rotor of CPM, (b) the stator of CPM (c) rotor of TFM, and (d) stator of TFM.

IV. Quantitative Comparison of Performance of Outer Rotor TFM and CPM

A. Topology of outer rotor CPM and TFM

Fig. 4 depicts the magnetic relevant parts of one stack of CPM and TFM. The three phase topology is completed by stacking the three single-phase stacks axially with angular shift of 120 electrical degrees. In the prototypes, the rotor and magnets of CPM and TFM will be stacked with no phase shifts, while the stator core will be shifted. Each stack has one global coil around the stator core, and the stator core is molded in two halves. Thus, a relatively high slot fill factor can be achieved in these motors, and the manufacturing cost is reduced.

The differences between these two motors are listed as: 1) For a 10 pole pairs motor, the CPM has 20 magnets in one stack, while the TFM has 40 magnets. 2) The stator core of the CPM is weaker than that of the TFM, as the claw is easy to break because the mechanical strength of the SMC is relatively low. 3) For the same volume, the coil window area of the CPM is smaller than that of the TFM.

Table IV lists the key dimensions and variables of CPM and TFM. To have a fair performance comparison, both of them have the same dimensions of the rotor outer radius, rotor inner radius, thickness of magnets, effective axial length, etc. Both of them use the same magnetic materials, which include the SMC, NdFeB, and electrical steels. As the structure of the CPM is more complex than that of TFM, the designed slot fill factor of the CPM is only 0.4 which is lower than the TFM's.

TABLE IV
KEY DIMENSIONS AND DESIGN VARIABLES OF CPM AND TFM

Dimension	CPM	TFM
Number of phases	3	3
Number of poles	20	20
Stator core material	SOMALOY™ 500	SOMALOY™ 500
Stator outer radius (mm)	40	40
Effective stator axial length (mm)	93	93
Rotor outer radius (mm)	47	47
Rotor inner radius (mm)	41	41
Permanent magnets	NdFeB, N30M	NdFeB, N30M
Number of magnets	60	120
Magnet dimensions	OD 88, ID 82, 31 mm, arc 12°	OD 88, ID 82, 9 mm, arc 12°
Magnetization direction	Radial	Radial
Main air gap length (mm)	1	1
Number of coils	3	3
Coil window dimension (mm^2)	15*16.5	15*20.5
Number of turns	80	125
Diameter of copper wire (mm)	1.25	1.25
Slot fill factor	0.4	0.5

B. Power equations of CPM and TFM

The flux linkage per coil for the CPM is

$$\varphi = \frac{B_{g\_cpm} 2\pi R_{so\_cpm} K_{sp\_cpm} L_{st2\_cpm} f(L_{st1\_cpm}, H_{st1\_cpm})}{2} \quad (27)$$

where R_{so_cpm} is the outer radius of stator, K_{sp_cpm} the claw pole arc ratio, L_{st2_cpm} the thickness of stator wall, and $f(L_{st1\_cpm}, H_{st1\_cpm})$ the effect of the claw pole dimension to flux per coil. The coil window area of CPM is

$$A_s = (L_{1\_cpm} - 2L_{st2\_cpm})(R_{so\_cpm} - R_{si\_cpm} - h_{st\_cpm} - h_{sy\_cpm}) \quad (28)$$

where L_{1_cpm} is the effective axial length of one disk, h_{st_cpm} the height of claw pole, and h_{sy_cpm} the length of stator yoke. The flux linkage per coil for the TFM is

$$\varphi = \frac{B_{g\_tfm} 2\pi R_{so\_tfm} K_{sp\_tfm} L_{st\_tfm}}{2} \quad (29)$$

where B_{g_tfm} is the air gap flux density of TFM, R_{so_tfm} the stator outer radius of TFM, K_{sp_tfm} the ratio of the stator tooth length in circumferential direction with respect to the pole arc, and L_{st_tfm} the stator tooth width. The coil window area of TFM is

$$A_s = (L_{1\_tfm} - 2L_{st\_tfm})(R_{so\_tfm} - R_{si\_tfm} - h_{sy\_tfm}) \quad (30)$$

where L_{1_tfm} is the axial length of one stack, and h_{sy_tfm} the stator yoke length of TFM. Combining (9), (27), (28), (29), and (30), the electromagnetic torque of CPM is

$$T = \frac{m}{2} P_r K_{sf} B_{g\_cpm} \pi R_{so\_cpm} K_{sp\_cpm} L_{st2\_cpm} f(L_{st1\_cpm}, H_{st1\_cpm}) (L_{1\_cpm} - 2L_{st2\_cpm})(R_{so\_cpm} - R_{si\_cpm} - h_{st\_cpm} - h_{sy\_cpm}) J_m \quad (31)$$

The electromagnetic torque for TFM is

$$T = \frac{m}{2} P_r K_{sf} B_{g\_tfm} \pi R_{so\_tfm} K_{sp\_tfm} L_{st\_tfm} (L_{1\_tfm} - 2L_{st\_tfm})(R_{so\_tfm} - R_{si\_tfm} - h_{sy\_tfm}) J_m \quad (32)$$

By comparing (31) and (32), it can be found that the main difference between the CPM and the TFM is caused by: 1) the claw pole of the CPM reduces coil window and increases the flux linkages per coil, and 2) the difference of the flux leakage situation. Thus, the accurate comparison should be completed by the numerical analysis method. Based on (31) and (32), it can be seen that the axial length of the stator tooth of CPM and TFM should be a quarter of the axial length of one disk. In this paper, the CPM and TFM were designed by following this guideline. The power equation shows the difference. However, the accurate effect of the claw pole in the CPM should be analyzed by more complicated methods, for example, the equivalent magnetic network and finite element method (FEM). In this paper, considering the 3D flux path of CPM and TFM, the 3D FEM is applied

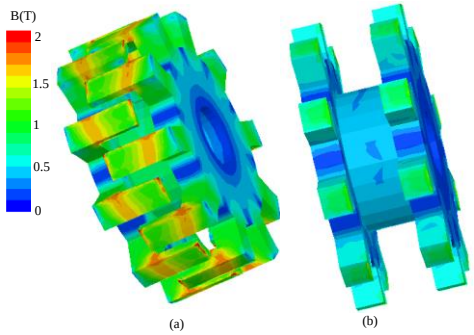

Fig. 5. Flux density distribution: (a) CPM, (b) TFM

C. 3D numerical field analysis

3D FEM is carried out to analyze the parameters of the motor. The flux density distribution in the stator core and air gap, the

inductance variation versus the rotor position, and cogging torque are analyzed by the commercial FEM software ANSYS.

Fig. 5 shows the flux density distribution of the CPM and TFM at no load situation. It can be found that the flux density of the CPM is quite high. The average flux density of its claw is around 1.0 T, and even reaches 1.8 T at the edge of the claw pole, while the flux density of the TFM is relatively low. The high flux density in the motor leads to relatively high torque ability, but it also brings the high core losses. To comprehensively compare the flux density of these motors, the air gap flux density at the radial direction is plotted, as shown in Fig. 6. The *x*-axis in the figure shows the electrical degree, the *y*-axis the position in the axial direction, and the *z*-axis the air gap flux density. It can be found that most fluxes provided by the magnets in CPM are utilized, while only half fluxes are used in the TFM. The air gap flux density of the CPM is higher than that of TFM.

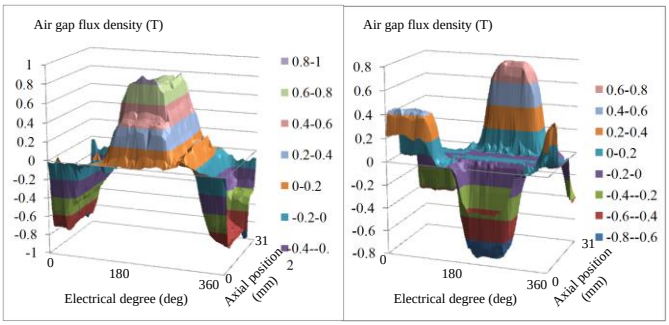

(a) (b)

Fig. 6. Air gap flux density in the radial direction: (a) CPM, and (b) TFM.

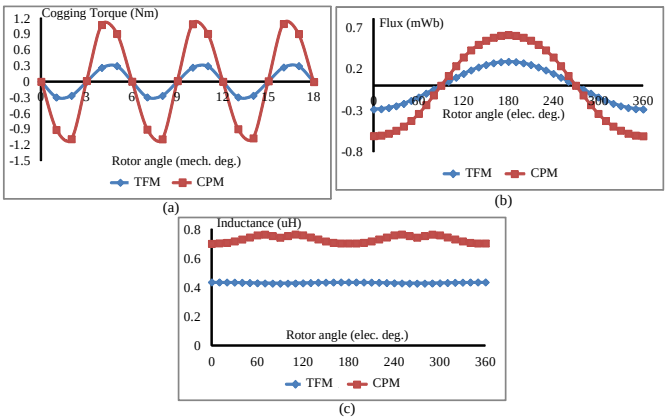

Fig. 7. 3D FEA results of CPM and TFM: (a) cogging torque, (b) no-load flux per turn of stator coil, and (c) inductance of per turn of stator coil.

D. Parameter analysis

Fig. 7 shows the 3D FEM analysis results of the CPM and TFM. Fig. 7(a) illustrates the cogging torque comparison (3 phases), where the cogging torque is calculated by using the Coulomb virtual work method in ANSYS. It can be found that the peak value of the cogging torque of CPM is 1.09 Nm, which is higher than that of TFM (0.326 Nm). Fig. 7(b) shows the stator winding flux per turn at the no-load, showing that the peak value of the CPM is 0.6084 mWb, and that of TFM is 0.2868 mWb. By differentiating the fluxes, the peak value of induced *emf* for the CPM and TFM is $0.0487\omega_r$ V, and $0.035\omega_r$ V respectively, where ω_r is the angular speed of the rotor with the unit of radian per second. Fig. 7(c) plots the inductance of these motors, showing that the average inductances per turn of the CPM and TFM are 0.734 and 0.433 μH respectively. Then, the overall inductance is 4.7 mH and 6.76 mH for the coils with 80 and 125 turns, respectively. As shown in Fig. 7(c), the inductance variation with the rotor position of the CPM is greater than the TFM's.

E. Loss analysis

Fig. 8 shows the no load core losses of stator core and rotor, and magnet loss of TFM and CPM. It shows that the core loss increases approximately linearly with the speed, while the magnet loss increases quadratically with the speed. The core loss of CPM is about double that of TFM. Compared with the core loss, the magnet loss is relatively low, but it is produced in very limited space, and thus results in relatively high temperature rise in the magnets, which may make the magnets irreversible demagnetized.

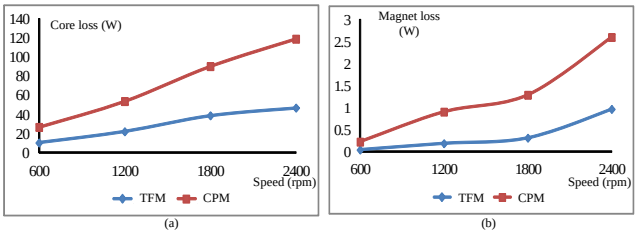

Fig. 8. No-load loss of TFM and CPM: (a) core losses, and (b) magnet eddy current loss.

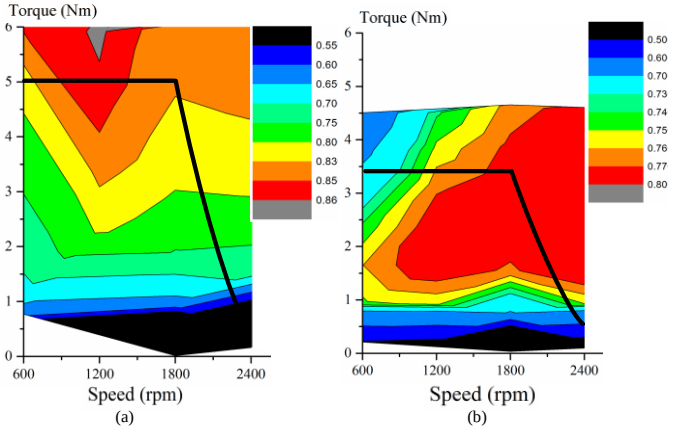

Fig. 9. Efficiency map, (a) CPM, (b) TFM

F. Performance prediction

To compare the performance, all motors should be operated with the same control method. In this paper, field oriented control method is applied for them, in which the phase current is controlled to be in the same phase as the back *emf* in the stator winding. In the modern electric drive system, the motor is generally operated at adjustable speed state, so it needs to know the motor's performance in different states. Thus, the efficiency map is a powerful method to shows its performance. The efficiency map of the CPM and TFM is shown in Fig. 9. In the map, the torque variation with the speed under the DC link voltage of 192 V is plotted. It shows that the CPM has higher torque ability, and higher efficiency.

V. Experiment Validation

To verify the effectiveness of the analysis results, the three phase TFM was tested, and some basic parameters and performance of TFM has been obtained.

A. Inductance and Resistance

At room temperature (20 °C), the stator winding resistance and inductance are measured. The resistance is measured by measuring the voltage of the winding, when 1 A DC current is input into the winding. The measured resistance is 0.305 Ω, while the calculated value is 0.31 Ω. A digital multifunctional meter, TES 2639 is used to measure the inductance. The measured inductance is 6.94 mH per turn, and the calculated value is 6.76 mH, which has a 3.5% relative error.

B. Back EMF and DC link voltage

When the motor operated as generator, which was driven by a DC motor, the back *emf* can be measured. The phase *emf* measured is $0.345\omega_r V$, which is 1.5 % lower than the calculated value $0.35\omega_r V$.

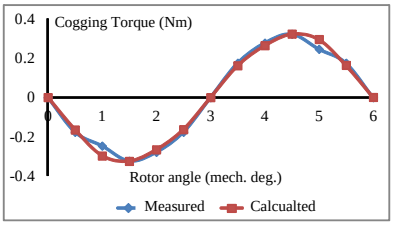

Fig. 10. Calculated and measured for TFM with three stack motor.

C. Cogging torque

To measure the cogging torque, the stator was fixed with a rotatable air bearing plate. By displacing the stator, the cogging torque can be measured by a spring balance which was connected with the air bearing plate. Fig. 10 plots the comparison between the measured cogging torque and the calculated value. The calculated peak value of the cogging torque of the TFM is 0.3256 Nm, while the measured peak value of the cogging torque is 0.32 Nm, the relative error between the calculated value and the experiment value is only 1.75%.

D. Core losses

By fitting the measured core loss and calculated loss,

$$P_{core} = c_h \omega_r + c_e \omega_r^2 \qquad (33)$$

it can be found that the c_h and c_e for the measured results are 0.01904 and $1.058e^{-4}$ respectively, and the c_h and c_e for the calculated results are 0.01976 and $1.156e^{-7}$ respectively. Compared the calculated results and experiment results, it can be seen that the hysteresis losses of the TFM has been predicted accurately, while the eddy current loss is not matched. The reason is that the eddy current loss also exists in the other part of the motor, such as the end caps, the inner electrical stainless steels between the adjacent stacks, and the magnets, which is not counted.

TABLE V
KEY MOTOR PARAMETERS

Parameter	Measured	Prediction
Motor back *emf* constant (V/rpm)	0.345	0.350
Phase resistance (Ω)	0.305	0.310
Phase inductance (mH)	6.94	6.76
Maximum cogging torque (Nm)	0.32	0.3256
Rated efficiency (%)	79.5	77.8

E. Summary of the Calculated Results and Experiment

Table V summaries the key parameter comparison between the calculated and experiment results; it can be seen that the analysis results of the TFM match well with the experiment ones.

VI. Summary of Comparison of CPM, TFM and RFM

As more PM materials are used in the CPM, it is necessary to consider the excessive material cost in this motor. In this paper, the material costs of main magnetic parts are considered, and it is estimated that the SMC is AUD 2 per kilogram, Coil is AUD 9 per kilogram, and NdFeB is AUD 100 per kilogram. The main material cost for the CPM is AUD 40, and the TFM is 30 AUD. The PM cost of the CPM is 32.2 AUD, which takes about 75% of the total most material cost of CPM. The main cost difference is due to the PM cost.

Table VI lists the main parameters comparison of CPM and TFM. It can be found that the torque density of the CPM is higher than that of TFM even with the slot fill factor of 0.4, which is lower than the 0.5 in TFM. Meanwhile, the CPM has the higher torque per cost than that of TFM. The CPM has higher efficiency than TFM; however, its cogging torque is higher too. Therefore, the overall performance of the CPM is better than TFM, except the cogging torque.

TABLE VI
COMPARISONS OF CPM AND TFM

Parameter	CPM	TFM
Rated output power (W)	942	640
Rated torque (Nm)	5.0	3.4
Rated Efficiency (%)	83	77
Cogging Torque maximum (Nm)	1.09	0.326
Slot fill factor	0.4	0.5
Rated current density (A/mm^2)	5.5	5.5
Torque per unit (Nm/m^3)	7747	5268
Cost (AUD)	40.05	29.5
Torque per cost (Nm/AUD)	0.125	0.103

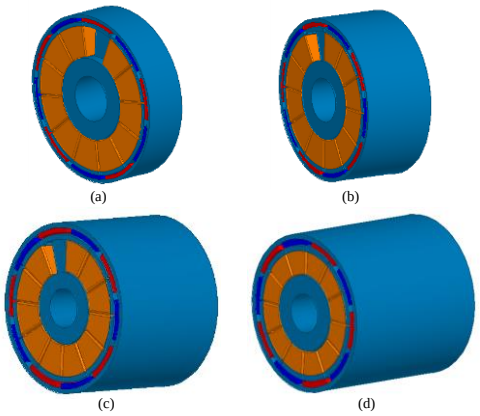

Fig. 11. Topology of outer rotor RFM with different ratio of axial length to outer radius, (a) 0.5, (b) 1, (c) 1.5 and (d) 2

Since the radial flux machine (RFM) is more popular than the CPM in the practical applications, it is necessary to compare the performance of the CPM with RFM. In this section, considering that the outer rotor RFM can output higher torque than the inner rotor RFM and the RFM with different ratio of axial length to outer radius will have different performance, the four kinds of outer RFM designs are optimized and compared with the CPM. For the best utilization of the magnetic isotropy property of SMC material, the stator teeth tips are extended both axially and circumferentially and the stator yoke is extended axially. Fig. 11 shows the main topology of outer rotor RFM with different ratios of axial length to outer radius, where the main magnetic volume is the same as the outer rotor CPM and TFM, the difference is the ratio of axial length to outer radius.

TABLE VII
COMPARISON OF CPM AND OUTER ROTOR RFM

Parameter	CPM	RFM			
		0.5	1	1.5	2
Rated output power (W)	942	675	880	634	475
Rated torque (Nm)	5.0	3.6	4.7	3.4	2.52
Rated efficiency (%)	83	86	88	84	80
Slot fill factor	0.4	0.5	0.5	0.5	0.5
Material cost (AUD)	40.05	47.97	60.53	55.78	59.77
Torque per cost (Nm/AUD)	0.125	0.075	0.077	0.061	0.042

By using the 3D FEM, the parameters and the performance of these machines can be obtained, as shown in Table VII. Compared with the outer rotor CPM which has the better performance than the outer rotor TFM, it can be seen that the torque ability of the outer RFM depends on the ratio of axial length to the outer radius, where it has been proven in Section III. For the RFM listed in the table, the one with $\lambda = 1$ has the best performance, which is similar to the inner rotor RFM designed in [17]. When comparing the output power, torque density, torque/cost, the CPM is the best choice. However, the efficiency of outer rotor RFM is 0.88 which is much higher than that of CPM. Thus, for specific applications, the CPM and RFM can be chosen in terms of user preferences and given requirements, for example, the volume.

VII. CONCLUSION

To investigate the performance of electrical machines with SMC cores for commercial production, it is necessary to know the differences among them. Five electrical machines with SMC cores developed in the last decades are compared in this work. To compare them fairly, some assumptions which include the temperature rise of coil, slot fill factor were made to be equal. It shows that the outer rotor CPM and outer rotor TFM are the better candidates to have SMC cores. A qualitative comparison among the AFM, RFM and TFM based on deduction of the equation of torque ability is also presented. It is found that the TFM is the best one for application of the high ratio of effective axial length to the motor outer radius, while the AFM and RFM are better for the low ratio of effective axial length to the motor outer radius applications. For the design of electrical machines with SMC cores, more attentions should be paid to the out rotor CPM and outer TFM with higher ratio of effective axial length to motor outer radius and higher number of pole pairs.

As the 3D flux electrical machine, the flux paths of CPM and TFM are very complicated. If they are designed with structure of outer rotor, they have higher torque ability than other structures. Thus, comprehensive comparison of outer rotor CPM and TFM has been done, based on the power equation and numerical analysis method. By comparing the cogging torque, performance, etc., it can be found that the outer rotor CPM has higher torque per unit volume, torque per cost, and higher efficiency. However, the cogging torque of CPM is higher than that of TFM.

Considering that the outer rotor RFM is a very general electrical machine used in the practical application, the comparison among four different outer RFM (optimized) and CPM is also addressed. It can be shown that the CPM is best for the torque density and torque/cost. However, the outer rotor RFM is better for the efficiency. The torque density of the outer rotor RFM with $\lambda = 1$ has the best performance.

In general, for the electrical machines with SMC cores, the outer rotor CPM can be considered to be the best for most situations. However, some further effective measures should be developed to decrease its cogging torque.

REFERENCE

[1] Y. G. Guo, J. G. Zhu, P. A. Watterson, and W. Wu, "Development of a PM transverse flux motor with soft magnetic composite core," *IEEE Trans. Energy Convers.*, vol. 21, pp. 426-434, 2006.

[2] A. G. Jack, B. C. Mecrow, C. P. Maddison, and N. A. Wahab, "Claw pole armature permanent magnet machines exploiting soft iron powder metallurgy," in *IEEE International Electric Machines and Drives Conference Record, 1997*. 1997, pp. MA1/5.1-MA1/5.3.

[3] Y. G. Guo, J. G. Zhu, and D. G. Dorrell, "Design and analysis of a claw pole permanent magnet motor with molded soft magnetic composite core," *IEEE Trans. Magn.*, vol. 45, pp. 4582-4585, 2009.

[4] G. Cvetkovski, L. Petkovska, M. Cundev, and S. Gair, "Improved design of a novel PM disk motor by using soft magnetic composite material," *IEEE Trans. Magn.*, vol. 38, pp. 3165-3167, 2002.

[5] R. Di Stefano and F. Marignetti, "Electromagnetic analysis of axial-flux permanent magnet synchronous machines with fractional windings with experimental validation," *IEEE Trans. Ind. Electron.*, vol. 59, pp. 2573-2582, 2012.

[6] The latest development in soft magnetic composite technology, http://www.hoganas.com

[7] Iron core material-Somaloy, http://www.hoganas.com

[8] J. Cros, P. Viarouge, Y. Chalifour, and J. Figueroa, "A new structure of universal motor using soft magnetic composites," *IEEE Trans. Ind. Appl.*, vol. 40, pp. 550-557, 2004.

[9] Y. G. Guo, J. G. Zhu, H. Y. Lu, Z. W. Lin, and Y. J. Li, "Core loss calculation for soft magnetic composite electrical machines," *IEEE Trans. Magn.*, vol. 48, pp. 3112-3115, 2012.

[10] T. Ishikawa, K. Takahashi, H. Q. Viet, M. Matsunami, and N. Kurita, "Analysis of novel brushless DC motors made of soft magnetic composite core," *IEEE Trans. Magn.*, vol. 48, pp. 971-974, 2012.

[11] Y. K. Huang, J. G. Zhu, Y. G. Guo, Z. W. Lin, and Q. S. Hu, "Design and analysis of a high-speed claw pole motor with soft magnetic composite core," *IEEE Trans. Magn.*, vol. 43, pp. 2492-2494, 2007.

[12] J. Cros, P. Viarouge, and M. T. Kakhki, "Design and optimization of soft magnetic composite machines with finite element methods," *IEEE Trans. on Magn.*, vol. 47, pp. 4384-4390, 2011.

[13] G. Cvetkovski and L. Petkovska, "Performance improvement of PM synchronous motor by using soft magnetic composite material," *IEEE Trans. Magn.*, vol. 44, pp. 3812-3815, 2008.

[14] G. Lei, T. S. Wang, J. G. Zhu, Y. G. Guo, and S. H. Wang, "System level design optimization methods for electrical drive systems: robust approach," *IEEE Trans. Ind. Electron.*, vol. 62, no. 8, pp. 4702-4713, Aug. 2015.

[15] Y. G. Guo, J. G. Zhu, P. A. Watterson, and W. Wu, "Comparative study of 3-D flux electrical machines with soft magnetic composite cores," *IEEE Trans. Ind. Appl.*, vol. 39, pp. 1696-1703, 2003.

[16] L. Ji-Young, K. Dae-Hyun, M. Seung-Ryul, and H. Choong-Kyu, "Design of an axial flux permanent magnet generator for a portable hand crank generating system," *IEEE Trans. on Magn.*, vol. 48, pp. 2977-2980, 2012.

[17] A. G. Jack, B. C. Mecrow, P. G. Dickinson, D. Stephenson, J. S. Burdess, N. Fawcett, *et al.*, "Permanent-magnet machines with powdered iron cores and prepressed windings," *IEEE Trans. Ind. Appl.*, vol. 36, pp. 1077-1084, 2000.

[18] M. Morimoto and M. Inanori, "Induction motor made of SMC," in *Proc. ECE-ASIA, International conference on power electronics*, Hiroshima, 2014. pp. 3509-3512.

[19] G. De Donato, F. G. Capponi, and F. Caricchi, "No-load performance of axial flux permanent magnet machines mounting magnetic wedges," *IEEE Trans. Ind. Electron.*, vol. 59, no. 10, pp. 3768-3779, Oct. 2012.

[20] B. Zhang, T. Seidler, R. Dierken, and M. Doppelbauer, "Development of a yokeless and segmented armature axial flux machine," *IEEE Trans. Ind. Electron.*, vol. 63, no. 4, pp. 2062-2071, Mar. 2016.

[21] J. Doering, G. Steinborn and W. Hodman, "Torque, power, losses, and heat calculation of a transverse flux reluctance machine with soft magnetic composite materials and disk shaped rotor," *IEEE Trans. Ind. Appl.*, vol. 51, no. 2, pp. 1494-1504, Mar./Apr. 2015

[22] O. Maloberti, R. Figueredo, C. Marchand, Y. Choua, D. Condamin, L. Kobylanski, *et al.*, "3-D & 2-D dynamic magnetic modeling of an axial flux permanent magnet motor with soft magnetic composites for hybrid electric vehicles," *IEEE Trans. Magn.*, vol. 50, pp. 1-11, 2014.

[23] F. Marignetti, V. Delli Colli, and S. Carbone, "Comparison of axial flux PM synchronous machines with different rotor back cores," *IEEE Trans. Magn.*, vol. 46, pp. 598-601, 2010.

[24] G. Lei, T. S. Wang, Y. G. Guo, J. G. Zhu, and S. H. Wang, "System level design optimization methods for electrical drive systems: deterministic approach," *IEEE Trans. Ind. Electron.*, vol. 61, no. 12, pp. 6591-6602, Dec. 2014.

[25] F. Marignetti, V. Delli Colli, and Y. Coia, "Design of axial flux PM synchronous machines through 3-D coupled electromagnetic thermal and fluid-dynamical finite-element analysis," *IEEE Trans. Ind. Electron.*, vol. 55, pp. 3591-3601, 2008.